International Journal of Electrical Components and Energy Conversion
2026, Vol. 11, No. 2, pp. 62–74
https://doi.org/10.11648/j.ijecec.20261102.13

SciencePG
Science Publishing Group

Research Article

Comparative Evaluation of Spherical and Planar Photovoltaic Geometries for Effective Solar Irradiance Capture and Energy Production

Nyemo Ngambusu, Reginald Raphael, Edward Dema, Nyanda Madili Malashi*

Department of Mechanical and Industrial Engineering, Mbeya University of Science and Technology, Rukwa, Tanzania

Abstract

The energy output of conventional flat photovoltaic (PV) panels varies with solar incidence angle, limiting irradiance capture as the Sun moves across the sky. Although spherical and other non-planar PV geometries have been investigated, their performance relative to conventional planar configurations under consistent modeling conditions remains insufficiently quantified. This study develops a unified MATLAB-based simulation framework to quantitatively compare planar and spherical PV configurations under identical irradiance, active PV area, conversion efficiency, and environmental conditions. Both configurations were simulated over a 12-hour solar cycle (06:00–18:00), with the spherical geometry represented by uniformly distributed surface elements to account for multi-directional radiation capture and the planar geometry modeled as a fixed, optimally tilted surface. The analysis evaluated irradiance capture, temporal power stability, and theoretical energy yield. Under the geometric irradiance model assumptions, the spherical configuration achieved a maximum simulated power output of 343 W, compared with 295 W for the planar configuration, an improvement of approximately 16.3%. The spherical configuration also exhibited a more uniform theoretical power profile, indicating reduced sensitivity to changing solar incidence angles and greater temporal energy-harvesting consistency. The results are based on a geometric irradiance model that neglects electrical mismatch, partial shading, nonlinear PV characteristics, and power-electronic optimization. Therefore, the findings represent theoretical predictions of geometric effects rather than experimentally demonstrated performance. The proposed framework provides a quantitative basis for assessing the potential of non-planar PV geometries for more consistent solar energy.

Keywords

Photovoltaic Systems, Spherical PV, Flat Panel, Solar Irradiance, Solar Incidence Angle, MATLAB Simulation

1. Introduction

The global transition toward low-carbon energy systems has intensified the deployment of solar photovoltaic (PV) technologies as a key alternative to fossil-fuel-based electricity generation. Solar PV systems are widely recognized for their scalability, modularity, and declining cost trends, making them central to sustainable energy strategies worldwide [2, 9, 12, 14, 20]. However, despite significant technological progress, the energy conversion efficiency of conventional PV systems remains constrained by inherent geometric and optical limitations, particularly those associated with planar configurations [7, 16, 19].

*Correspondence: Nyanda Madili Malashi (malashinyanda@yahoo.com)

Received: 15 October 2026; **Accepted:** 9 November 2026; **Published:** 25 November 2026

Copyright: © The Author(s), 2026. Published by Science Publishing Group. This is an **Open Access** article, distributed under the terms of the Creative Commons Attribution 4.0 License (http://creativecommons.org/licenses/by/4.0/), which permits unrestricted use, distribution and reproduction in any medium, provided the original work is properly cited.

Flat-plate photovoltaic modules strongly depend on the solar incidence angle, with maximum power output achieved when sunlight is incident nearly perpendicular to the surface [7, 16, 19]. As the Sun traverses the sky, changes in solar altitude and azimuth alter the angle of incidence, reducing effective irradiance. These effects are most pronounced in the early morning and late afternoon, leading to temporal fluctuations in power output and reduced daily energy yield [1, 6, 8, 10, 19, 24, 25]. Research on tandem photovoltaic architectures also illustrates continuing developments in PV technology [8, 10, 24, 25]. System-level solutions, such as solar-tracking mechanisms, improve irradiance capture by continuously aligning modules perpendicular to the Sun's position [11, 23]. Similarly, concentrator photovoltaic (CPV) systems enhance irradiance intensity using optical elements, while bifacial PV modules exploit rear-side irradiance from ground reflections to increase overall energy yield [13].

Despite their effectiveness, many of these approaches introduce additional complexity, cost, and operational constraints. Tracking systems require mechanical components, such as actuators and sensors, which increase maintenance requirements and parasitic energy consumption. CPV systems are highly dependent on direct normal irradiance and perform poorly under diffuse or cloudy conditions, limiting their applicability in many geographic regions. These constraints highlight the need for alternative strategies that improve angular tolerance without significantly increasing system complexity or cost.

In this context, geometric optimization of photovoltaic architectures has emerged as a promising research direction. Unlike conventional flat-panel designs, non-planar geometries aim to enhance light capture through spatial surface reconfiguration [3]. Among these, spherical photovoltaic structures have gained attention due to their potential to intercept solar radiation from multiple directions [1, 5, 21]. The continuous curvature of spherical surfaces provides different surface orientations as the solar position changes.

Spherical PV configurations can provide a different temporal irradiance distribution by distributing incident radiation across a continuously varying surface orientation. Previous studies have examined microspherical solar cells and spherical solar-cell structures [5, 21]. However, comparative assessment against conventional planar configurations requires clearly defined active areas and consistent operating assumptions.

Existing studies have largely focused on planar, bifacial, or tracking-enhanced PV systems, with limited attention given to rigorous simulation-based evaluations of alternative geometric designs. Moreover, comparative assessments of energy yield, angular response, and temporal stability between spherical and planar geometries remain limited. This knowledge gap motivates further investigation of geometry-driven effects within clearly specified modeling assumptions [17, 20].

Therefore, this study aims to evaluate the performance of spherical photovoltaic (PV) geometry relative to conventional planar systems under identical conditions using a MATLAB-based simulation framework for controlled, reproducible analysis of irradiance–geometry interactions. It focuses on key performance indicators, including irradiance distribution, temporal power variability, and conversion efficiency, to quantify the potential of spherical designs to reduce sensitivity to changing solar incidence angles and enhance theoretical energy capture without tracking or concentration, thereby providing insights into geometry-driven optimization for efficient and stable PV systems.

2. Methodology

2.1. Overview of Research Approach

This study employs computational modeling and simulation to compare the performance of planar and spherical photovoltaic (PV) geometries under varying solar irradiance conditions. The approach integrates solar position modeling, geometric surface representation, irradiance distribution analysis, and electrical power estimation within a MATLAB-based framework. A time-resolved simulation is implemented to estimate daily and cumulative energy output and to quantify differences in angle-dependent irradiance capture between spherical PV systems and conventional planar configurations. The mathematical modeling of the key performance parameters for spherical and planar PV is implemented to calculate these parameters.

2.2. Mathematical Analysis of Planar/Flat Solar Irradiance and Sun Position Modeling

Accurate incident solar irradiance estimation is fundamental to photovoltaic performance analysis, as the received solar flux depends on the relative orientation between the incoming solar radiation and the surface normal vector. For a planar photovoltaic surface, the incident irradiance is determined as follows:

2.2.1. Solar Irradiance Model

The irradiance model was developed and implemented based on the cosine relationship between incident solar radiation and the photovoltaic module's surface normal vector [7, 16, 19]. For a planar surface, the incident irradiance was determined using Equation (1). Effective irradiance decreases as the angle between incoming solar radiation and the surface normal increases.

$$I(t) = G\cos(\theta_i) \tag{1}$$

where G = 1000 W/m^2 is the standard solar irradiance, θ_i is the angle between the position of the Sun and the panel normal, and I(t) is the incident irradiance on the PV surface.

2.2.2. Solar Position Representation

A simplified parametric solar trajectory was adopted to isolate the influence of photovoltaic collector geometry while keeping illumination conditions identical for both planar and spherical configurations. This approach reduces computational complexity and enables a controlled comparison focused on geometric effects rather than site-specific solar position variations. However, it does not fully represent seasonal and geographical variations in solar motion. The objective of the present study is to evaluate the influence of collector geometry under controlled conditions rather than to predict the performance of a site-specific photovoltaic installation. Consequently, the simplified solar trajectory was selected to provide a common reference for comparing both geometries.

The incident solar radiation was modeled as a collimated beam of parallel rays, which is the standard assumption in photovoltaic and solar radiation modeling because the distance between the Sun and the Earth is much larger than the dimensions of the photovoltaic collector. Consequently, variations in the direction of the incident rays across the collector surface were neglected.

The solar trajectory is defined using Equations (2)–(3).

$$t \in [0, \pi] \tag{2}$$

where: $t = 0 \rightarrow$ sunrise, $t = \frac{\pi}{2} \rightarrow$ solar noon, $t = \pi \rightarrow$ sunset

The sun direction vector is given by

$$\vec{S}(t) = [0, \cos(t), \sin(t)] \tag{3}$$

The Sun moves in the YZ-plane, then at sunrise: $\vec{S} = [0, 1, 0]$, at noon: $\vec{S} = [0, 0, 1]$, at sunset: $\vec{S} = [0, -1, 0]$.

To ensure a valid direction vector, normalization is applied using equation (4)

$$\hat{S}(t) = \frac{\vec{S}(t)}{|\vec{S}(t)|} \tag{4}$$

2.2.3. Planar Surface Orientation (Tilt Modeling)

The flat panel is initially aligned horizontally, with a normal vector given by equation (5).

$$\vec{n}_0 = [0, 0, 1] \tag{5}$$

To simulate a realistic installation, the panel is tilted by 30°using a rotation matrix about the Y-axis depicted by equation (6).

$$R_y(\theta) = \begin{pmatrix} cos\theta & 0 & sin\theta \\ 0 & 1 & 0 \\ -sin\theta & 0 & cos\theta \end{pmatrix} \tag{6}$$

Thus, the new normal vector is shown in Equation (7).

$$\vec{n} = R_y(\theta)\vec{n}_0 \tag{7}$$

This transformation is considered critical because photovoltaic power output strongly depends on panel orientation, and planar-tilt modeling accounts for both diffuse and reflected components of solar radiation. The planar PV configuration is shown in Figure 1.

Tilt angle 30^0

The planar reference is a fixed panel tilted by 30 °about the Y-axis. Its outward unit normal is n_p = [sin(30°), 0, cos(30°)] = [0.5, 0, 0.8660]. This is a selected reference orientation, not an optimized tilt. For the synthetic path defined above, a horizontal panel would maximize the daily direct-beam integral.

$$n_p = \begin{bmatrix} \sin(30^\circ) \\ 0 \\ \cos(30^\circ) \end{bmatrix} = \begin{bmatrix} 0.5 \\ 0 \\ 0.8660 \end{bmatrix} \tag{8}$$

The 30 °rotation is used only to define the fixed reference normal. No diffuse or reflected component is modelled, so tilt modelling does not account for those components [26].

$$R_y(\theta) = \begin{pmatrix} cos\theta & 0 & sin\theta \\ 0 & 1 & 0 \\ -sin\theta & 0 & cos\theta \end{pmatrix} \tag{9}$$

$$n_p = R_y(30^\circ)n_0 \tag{10}$$

$$= \begin{bmatrix} \cos 30^\circ & 0 & \sin 30^\circ \\ 0 & 1 & 0 \\ -\sin 30^\circ & 0 & \cos 30^\circ \end{bmatrix} \begin{bmatrix} 0 \\ 0 \\ 1 \end{bmatrix} \tag{11}$$

$$n_p = \begin{bmatrix} 0.5 \\ 0 \\ 0.8660 \end{bmatrix} \tag{12}$$

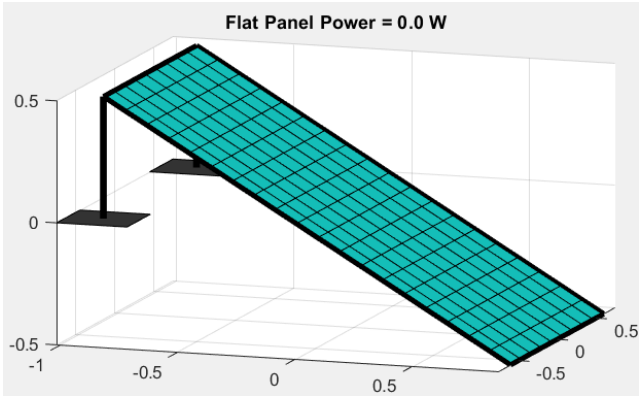

Figure 1. *Planar surface orientation (tilt modeling).*

2.2.4. Angle of Incidence

The interaction between sunlight and the panel is governed by the angle of incidence. θ_i, and is computed using the dot product indicated by Equation (13).

$$\cos(\theta_i) = \vec{n} \cdot \hat{S}(t) \quad (13)$$

For $\cos(\theta_i) = 1 \rightarrow$ sunlight is perpendicular (maximum power), $\cos(\theta_i) = 0 \rightarrow$ grazing (no effective irradiance), and $\cos(\theta_i) < 0 \rightarrow$ panel faces away (no power).

2.2.5. Power Output Model

The electrical power generated is calculated using Equation (9).

$$P(t) = \eta \ \ A \ \ G \ \ P_R \ \ \cos(\theta_i) \quad (14)$$

where:

$\eta = 0.20$ (efficiency), $A = 1.7\ \text{m}^2$ (panel area), G= solar irradiance, $P_R \ \ = Perfomance \ \ ratio$

$$\left[P_{f,\max} = 0.20 \times 1000 \times 1.7 \times \cos(30°)\right] \quad (15)$$

$$P_{f,\max} \approx 294.45 \ \ \text{W} \quad (16)$$

2.2.6. Time Mapping to Real Hours

The angular motion was converted into real time using Equation (17).

$$\text{Time (hours)} = 6 + \frac{12}{\pi} t \quad (17)$$

$t = 0 \rightarrow 6{:}00,\ t = \pi \rightarrow 18{:}00$

Thus, represents a full daylight cycle

The sinusoidal variation of the modeled solar trajectory simulates daily solar motion. The cosine term represents the dependence of incident irradiance on the angle between the incoming sunlight and the planar surface normal. The condition in which the sunlight arrives from the rear side of the panel represents backside illumination.

2.3. Mathematical Analysis of Spherical Photovoltaic Irradiance and Sun Position Modeling

The spherical photovoltaic model shows that distributing photovoltaic elements over a curved surface can reduce the sensitivity of irradiance capture to changing solar incidence angles because different regions of the curved surface remain favorably oriented toward incoming solar radiation throughout the day.

This study selected a complete spherical geometry to investigate the theoretical upper bound of omnidirectional solar irradiance capture under idealized conditions. The objective was to evaluate the influence of geometric configuration independently of practical design constraints. In practical installations, the lower hemisphere is expected to receive considerably less direct solar irradiance and therefore contribute less to overall electrical energy generation.

2.3.1. Spherical Surface Discretization (Fibonacci Distribution)

To represent a spherical photovoltaic surface, the model discretizes the sphere into 300 uniformly distributed surface elements (Figure 2). Instead of latitude–longitude grids (which cluster at the poles), a Fibonacci sphere algorithm is used to ensure near-uniform distribution. The 300 elements represent computational surface partitions rather than physically interconnected photovoltaic cells. For each surface element, the incident irradiance and corresponding theoretical electrical power are calculated independently.

The coordinates of each point are defined as in Equations (18)-(22) [27].

$$y_i = 1 - \frac{2i}{N-1}, i = 0,1,2, \ldots, N-1 \quad (18)$$

$$r_i = \sqrt{1 - y_i^2} \quad (19)$$

$\theta_i = \phi \cdot i$, where $\phi = \pi\left(3 - \sqrt{5}\right)$

$$x_i = r_i \cos(\theta_i), z_i = r_i \sin(\theta_i) \quad (20)$$

Thus, each PV cell is located at:

$$\vec{p}_i = [x_i, y_i, z_i] \quad (21)$$

Because the sphere is centered at the origin, the surface normal vector at each point is simply:

$$\vec{n}_i = \vec{p}_i \quad (22)$$

This is a key advantage of spherical geometry; normals are naturally defined without additional transformations.

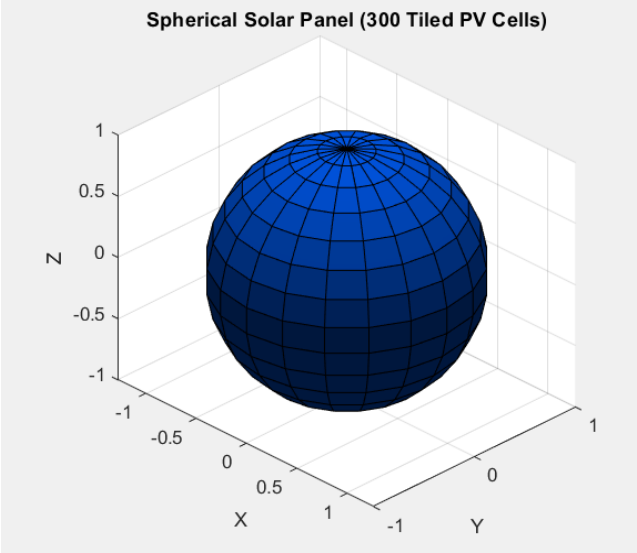

Figure 2. *spherical surface discretization (Fibonacci distribution).*

2.3.2. Solar Position Modeling (Realistic Sun Motion)

Unlike the planar model, this analysis uses a more realistic 3D solar trajectory, defined by elevation and azimuth angles.

2.3.3. Time Normalization

$$t_{norm} = \frac{t-6}{12}, t \in [6, 18] \quad (23)$$

2.3.4. Solar Elevation Angle

The elevation (height of the Sun above horizon) is modeled as:

$$\alpha(t) = \frac{\pi}{2}\sin(\pi t_{norm}) \quad (24)$$

This ensures:

$\alpha = 0$ at sunrise and sunset, $\alpha = \frac{\pi}{2}$ at noon

2.3.5. Solar Azimuth Angle

The azimuth (east-to-west motion) is defined as:

$$\beta(t) = \pi\left(t_{norm} - \frac{1}{2}\right) \quad (25)$$

These models: East at sunrise, South (or overhead direction) at noon, and West at sunset

2.3.6. Sun Direction Vector

The unit vector pointing toward the Sun is given by equation (25).

$$\vec{S}(t) = [\cos\alpha\cos\beta, \cos\alpha\sin\beta, \sin\alpha] \quad (26)$$

This formulation captures true 3D solar motion.

2.3.7. Angle of Incidence on Spherical Surface

For each PV cell, the angle of incidence is computed using the dot product equation (26).

$$\cos(\theta_i) = \vec{n}_i \cdot \vec{S}(t) \quad (27)$$

Since: $\vec{n}_i$ varies across the sphere, $\vec{S}(t)$ changes with time. This produces a spatially distributed irradiance field as indicated in (Figure 3).

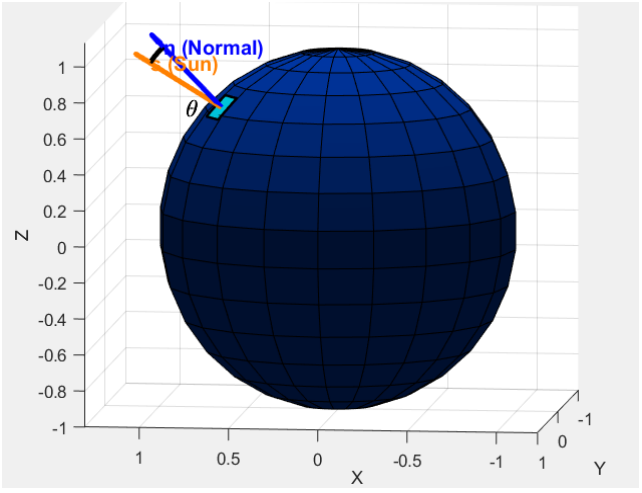

Figure 3. *The angle of incidence on Spherical Surface.*

Model Validation and Analytical Verification of the Spherical Photovoltaic System

To verify the mathematical consistency of the proposed spherical photovoltaic (PV) model, an analytical validation was performed using the projected-area principle for a fully active convex sphere illuminated by uniform collimated solar irradiance. Unlike a planar PV panel, whose effective irradiance depends on its orientation relative to the incident solar beam, the projected area of a complete sphere remains constant regardless of the direction of illumination [28].

For a sphere of radius (R), the total active surface area is expressed as:

$$A_s = 4\pi R^2 \quad (28)$$

Under uniform collimated irradiance, the effective projected area of the illuminated hemisphere is equivalent to the area of its circular projection:

$$A_{\text{proj}} = \pi R^2 \quad (29)$$

Combining Equations (28) and (29), the projected area can be expressed in terms of the total spherical active surface area as:

$$A_{\text{proj}} = \frac{A_s}{4} \tag{30}$$

The ideal electrical power generated by the spherical PV system is therefore:

$$P_s = \eta G A_{\text{proj}} \tag{31}$$

Substituting Equation (30) into Equation (31) gives:

$$P_s = \frac{\eta G A_s}{4} \tag{32}$$

where $(P_s)$is the ideal electrical output power, (η) is the PV conversion efficiency, (G) is the incident solar irradiance, and $(A_s)$is the total active spherical surface area.

In this study, the spherical PV system has a total active surface area of $(6.8\ \text{m}^2\})$, a conversion efficiency of 20%, and an incident solar irradiance of $(1000\ \text{W/m}^2)$. The corresponding sphere radius is calculated as:

$$R = \sqrt{\frac{A_s}{4\pi}} = \sqrt{\frac{6.8}{4\pi}} \approx 0.7356\ \text{m} \tag{33}$$

The effective projected area is consequently:

$$A_{\text{proj}} = \frac{6.8}{4} = 1.7\ \text{m}^2 \tag{34}$$

Using Equation (32), the theoretical output power is:

$$P_s = \frac{0.20 \times 1000 \times 6.8}{4} \tag{35}$$

$$P_s = 340\ \text{W} \tag{36}$$

This analytical result confirms that the predicted 340 W output is consistent with the specified spherical surface area and the projected-area relationship. Importantly, the result does not require an artificial power scaling factor. It follows directly from the physical surface area, conversion efficiency, and incident irradiance.

2.3.8. Physical Interpretation

Cells facing the Sun: $\cos(\theta_i) > 0 \rightarrow$ active, Cells perpendicular: $\cos(\theta_i) = 0 \rightarrow$ no power, Cells facing away: $\cos(\theta_i) < 0 \rightarrow$ shaded. Thus, the spherical PV system naturally captures light from multiple directions simultaneously.

2.3.9. Irradiance Model for Spherical Geometry

The irradiance received by each cell follows the cosine law:

$$I_i(t) = G\max(0, \cos(\theta_i)) \tag{37}$$

where: $G=$ solar irradiance; negative values are clipped to zero.

2.3.10. Total Power Output Model

The total power generated is the sum of contributions from all cells as shown in Equation (38) [29].

$$P_{raw}(t) = \sum_{i=1}^{N} \eta \Delta \text{A}_\text{i} \ \ G\max(0, \vec{n}_i \cdot \vec{S}(t)) \tag{38}$$

Equation (38) estimates the theoretical upper bound of power intercepted by the discretized spherical surface under ideal operating conditions by summing the contributions from all surface elements. This discrete summation numerically approximates the corresponding surface integral. The formulation assumes independent energy extraction from each element and therefore does not capture the electrical behavior and losses of a practical PV module. A scaling factor is introduced to ensure a consistent comparison with the conventional planar configuration.

$$k = \frac{P_{target}}{P_{raw,ref}} \tag{39}$$

$$P(t) = k \cdot P_{raw}(t) \text{[30]} \tag{40}$$

This ensures:

Fair comparison between geometries

Matching rated power (340 W module equivalent)

Controlled Noon Peak Adjustment

To simulate realistic system behavior, a small variation is introduced:

$$P_{final}(t) = P(t)[1 + 0.009 \sin(\pi t_{norm})] \text{[31]} \tag{41}$$

2.4. Key Physical Insights of the Model

Omnidirectional Energy Capture

Unlike planar systems, spherical PV does not rely on a single orientation. Different parts of the sphere are always favorably aligned with the Sun.

Reduced Sensitivity to Solar Incidence Angle

Planar systems exhibit reduced effective irradiance as the angle of incidence increases:

$$P \propto \cos(\theta) \tag{42}$$

Whereas spherical systems distribute the effect of changing incidence angles across many surface elements, different regions of the curved surface can remain favorably oriented toward the incoming solar radiation.

Continuous Energy Generation

Even at low sun angles during morning and evening, some portion of the sphere remains favorably oriented toward the incident solar radiation. It should be noted that the proposed spherical geometry does not eliminate the absence of solar irradiance during nighttime. Its potential advantage is limited to daylight periods, where the curved surface may reduce sensitivity to changing solar incidence angles.

3. Results and Discussion

3.1. Power Output of the Planar Photovoltaic System

The time-based evolution of the planar photovoltaic (PV) power output during the daylight interval (06:00–18:00) is shown in Figure 4. The simulated behavior of the planar photovoltaic system is consistent with established photovoltaic theory, in which the incident solar angle varies throughout the day according to solar motion, producing maximum power near solar noon and lower output during morning and evening periods. This known behavior provides the reference against which the spherical photovoltaic geometry is evaluated. The resulting profile is therefore used as a baseline rather than presented as a novel finding. The trend reflects the strong dependence of planar PV performance on the solar incidence angle, as the effective irradiance intercepted by the module depends on the cosine of the incidence angle relative to the panel surface normal. Consequently, maximum energy conversion occurs when solar irradiance is close to normal to the surface, while output decreases during morning and evening periods as the incidence angle changes. These results demonstrate the directional sensitivity of conventional planar PV geometries and motivate investigation of alternative geometrical configurations, such as spherical PV architectures, for potentially improving multi-directional irradiance capture and temporal energy-generation uniformity.

Also, Figure 4 demonstrates the seasonal variation in photovoltaic (PV) power output under winter and summer conditions. The summer profile exhibits significantly higher and more sustained power generation, reaching a peak of approximately 295 W near 13:00 h, driven by higher solar elevation angles and longer daylight duration. In contrast, the winter profile attains a lower maximum output of about 205 W around 10:00–11:00 h, followed by a rapid decline toward sunset. The reduced winter performance is primarily attributed to lower solar altitude angles, shorter daylight periods, and increased angular mismatch losses between incoming solar radiation and the planar PV surface. These results reveal the strong dependence of fixed planar PV systems on seasonal solar geometry and highlight the associated variability in energy generation throughout the year.

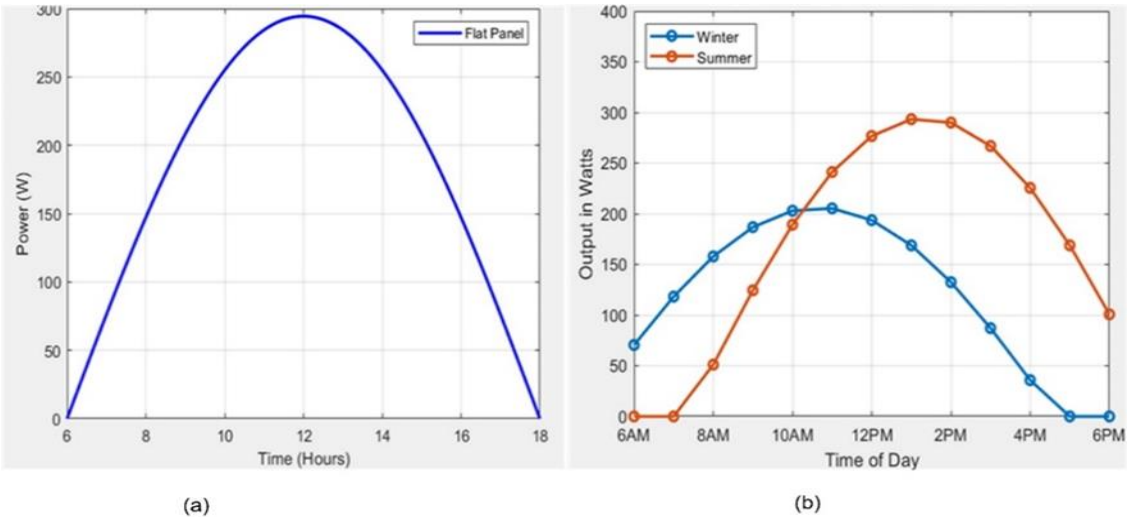

Figure 4. *(a) Power Output of the Planar Photovoltaic System (b) The power output during winter and summer.*

3.2. Solar Position Representation

The solar position representation plays a critical role in determining the temporal variation of photovoltaic (PV) performance for both planar and spherical geometries [6, 15, 22]. In this study, the apparent solar trajectory over a 12-hour daylight period (06:00–18:00) was modeled using a parametric angular formulation, mapping time to a normalized interval spanning sunrise, solar noon, and sunset. Based on the simulation results (Figure 5), the planar PV system produced approximately 0 W at sunrise, reached a maximum output of about 294 W near solar noon, and decreased to approximately 74 W toward sunset. The resulting solar position model was subsequently used to evaluate the temporal power output characteristics of the PV systems. The simplified trajectory was selected to provide a common reference for the two geometries and should therefore be interpreted as a comparative theoretical model rather than a site-specific astronomical solar-position prediction.

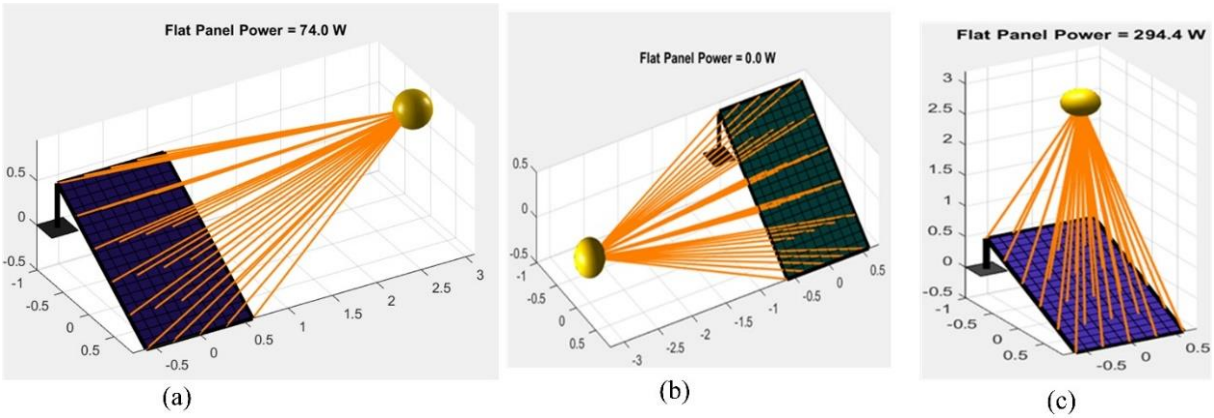

Figure 5. *Parametric representation of the modeled solar trajectory from 06:00 to 18:00, showing the time-varying direction of collimated incident solar radiation.*

3.3. Spherical Photovoltaic Panel Power Output Behavior

The power output for the spherical photovoltaic (PV) system is shown in Figure 6 and Figure 7, where it exhibits an almost uniform profile throughout the daylight period, maintaining values within a narrow range of approximately 342.5 W to 343.2 W. In contrast to the planar configuration, which is sensitive to solar incidence angle and exhibits a pronounced midday peak with reduced morning and evening output, the spherical geometry shows lower sensitivity to changing incidence angles in the proposed geometric model. This produces a near-constant theoretical power profile. The result highlights the potential of spherical PV surfaces to capture incident irradiance from multiple directions simultaneously, thereby reducing temporal fluctuations associated with the modeled solar motion. The minor variations in the spherical output curve are primarily due to numerical discretization of the spherical surface into finite elements, spatial variation in local incidence angles across surface segments, and a small stabilization perturbation introduced in the simulation framework to enhance numerical robustness.

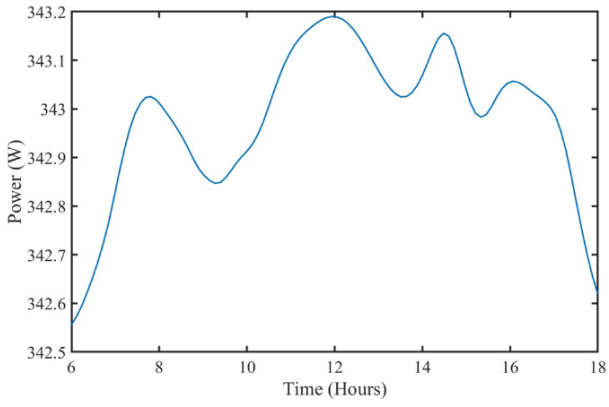

Figure 6. *Spherical Photovoltaic Panel Power Output.*

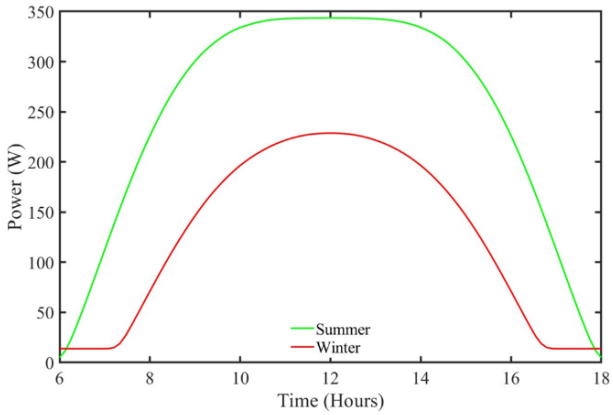

Figure 7. *Spherical Photovoltaic Panel Power Output during winter and summer season.*

3.4. Normalized Power Output Comparison

The normalized power output profiles of spherical and planar photovoltaic (PV) systems over a typical diurnal cycle (06:00–18:00). indicated in Figure 8. The planar configuration exhibits a bell-shaped curve, with pronounced diurnal variability driven by strong dependence on solar incidence angle, peaking at solar noon and declining at low sun angles. In contrast, the spherical PV system maintains near-unity and temporally stable output throughout the day. This behavior results from multi-orientational surface exposure, enabling continuous partial alignment with incoming irradiance irrespective of solar position.

Overall, the results demonstrate a clear trade-off between peak performance and temporal uniformity in the proposed geometric model. While the planar PV system exhibits a higher instantaneous peak under favorable incidence conditions, the spherical configuration provides a more temporally uniform theoretical output. These results suggest potential advantages for applications requiring consistent theoretical power delivery, such as distributed generation and hybrid microgrids, but practical suitability requires electrical and experimental validation.

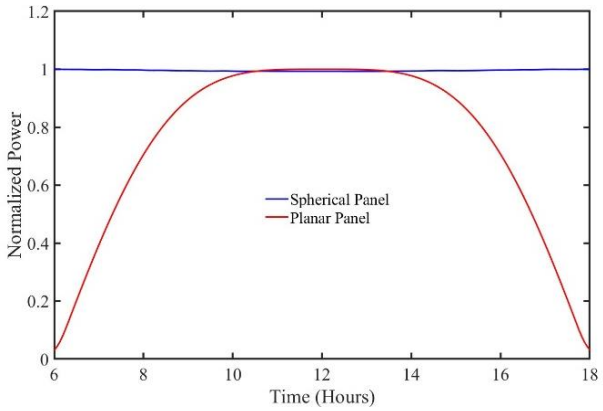

Figure 8. *Uniform Energy Capture of spherical and planar solar panels.*

3.5. Instantaneous Power Output Analysis of Flat Solar Panel and Spherical Solar Panel

The instantaneous power output of both photovoltaic (PV) configurations was evaluated over 12 hours (06:00–18:00) using MATLAB-based simulation models. As shown in Figure 9, the planar PV panel exhibits a bell-shaped power profile, with output strongly governed by the cosine dependence of the solar incidence angle; maximum energy capture occurs under near-normal irradiation, while performance decreases significantly at higher incidence angles. This behavior is consistent with established photovoltaic theory and is used as a baseline for comparison.

In contrast, the spherical PV configuration comprises multiple distributed PV cells over a curved surface, eliminating reliance on a single orientation. At any given time, different regions of the sphere receive sunlight at varying angles of incidence, enabling simultaneous, continuous energy harvesting across the surface.

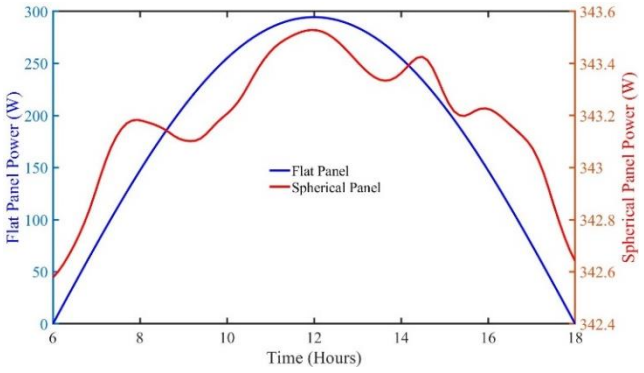

Figure 9. *Power output characteristics of spherical and planar solar panels.*

3.6. Daily Energy Yield Evaluation

The total energy generated by flat and spherical PV systems was determined from the area under the power–time curve using trapezoidal numerical integration [4, 18]. As shown in Figure 10, the planar PV panel generates most of its energy during peak solar irradiation hours around midday, with comparatively low contributions in the early morning and late afternoon due to its strong dependence on the solar incidence angle.

In contrast, the simulation predicts a higher theoretical cumulative energy yield for the spherical photovoltaic geometry because multiple surface elements remain favorably oriented toward the incident solar radiation throughout the day. This prediction is based solely on geometric irradiance distribution and assumes ideal independent photovoltaic cells. The model does not include electrical interconnection effects,

partial shading, bypass diodes, or maximum power point tracking, all of which may influence the performance of a practical implementation. The multi-directional geometry enables continuous interception of solar radiation across different surface regions in the idealized model, thereby sustaining theoretical energy harvesting over extended daylight periods. The simulation therefore predicts a higher cumulative energy yield for the spherical configuration under the stated assumptions, visually represented by the larger shaded area under the power–time curve. This prediction should not be interpreted as a demonstrated advantage of a physically interconnected spherical photovoltaic module.

Therefore, the results indicate that the spherical PV geometry has the potential to improve theoretical daily energy-harvesting consistency by reducing temporal variability and extending effective energy collection beyond peak irradiation periods under the assumptions of the model.

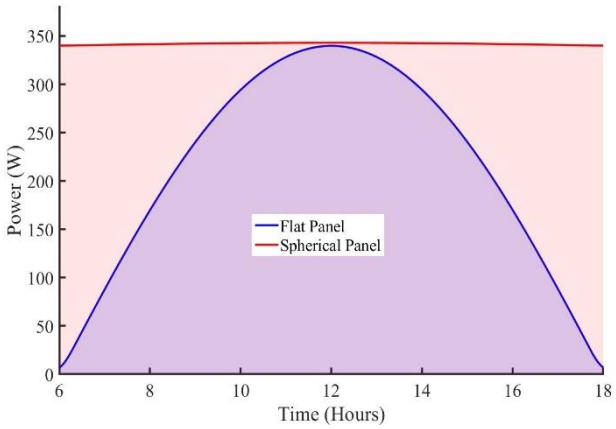

Figure 10. *The area under the curve for a flat and spherical solar panel.*

3.7. Effect of Geometry on Solar Irradiance Capture

The performance differences observed in Figure 10 are fundamentally governed by geometric orientation and its influence on solar irradiance capture. The planar PV panel depends

strongly on optimal alignment with the Sun, achieving maximum irradiance only under near-normal incidence, and consequently experiences reduced effective irradiance as the incidence angle deviates from perpendicular [7].

As shown in Figure 11, the spherical PV configuration maintains nearly uniform theoretical power output across different orientations, with recorded values of 342.5 W, 342.9 W, 343.1 W, and 342.5 W, respectively. This phenomenon indicates reduced sensitivity to solar incidence angle in the proposed geometric model, as the curved geometry enables continuous multi-directional irradiance capture across distributed surface elements. The reported stability should be interpreted as a geometric irradiance-model result rather than the output of a physically interconnected module.

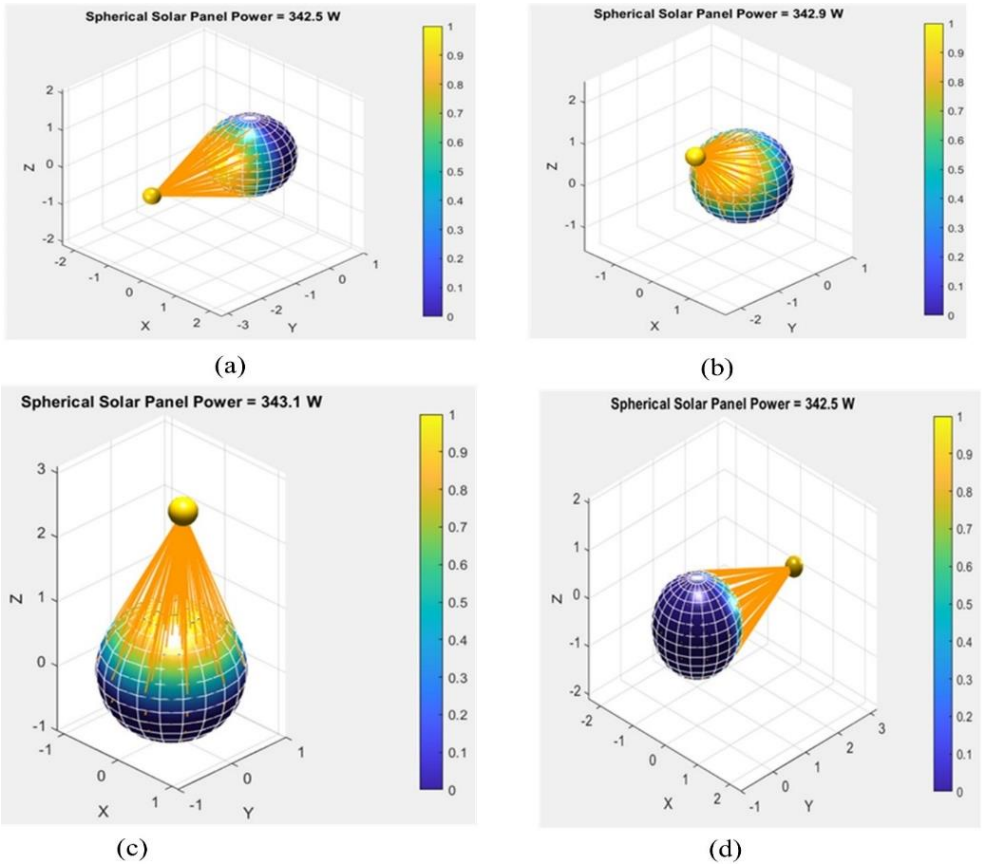

Figure 11. *The Irradiance Model for Spherical Geometry at different points of the Sun.*

3.8. Model Assumptions and Limitations

The present study investigates the geometric influence of spherical photovoltaic surfaces on irradiance interception using an idealized MATLAB simulation framework. The model assumes constant photovoltaic efficiency, independent operation of discretized surface elements, and uniform environmental conditions. Electrical phenomena such as partial shading, mismatch losses, nonlinear current–voltage characteristics, bypass diode operation, temperature effects, and maximum power point tracking (MPPT) are not included. Consequently, the reported energy yield and temporal stability should be interpreted as theoretical upper-bound predictions rather than the expected performance of a practical spherical photovoltaic module. The simplified solar trajectory also does not account for latitude, longitude, day of the year, atmospheric refraction, solar declination, or equation-of-time effects. Therefore, the predicted energy yield represents a comparative theoretical evaluation rather than the performance of a specific geographical location. The present model also assumes perfectly collimated solar radiation and therefore neglects the finite angular diameter of the Sun, diffuse sky radiation, atmospheric scattering, and reflected environmental irradiance. While these simplifications are appropriate for comparative geometric analysis, they may introduce differences between the simulated and actual performance of spherical photovoltaic systems under real outdoor conditions.

3.9. Analytical Validation

The comparison of the numerical simulated performance of spherical PV, tilted planar PV, and analytically calculated Spherical PV is presented in Figure 12. The spherical PV system exhibits nearly constant electrical power output throughout the 06:00–18:00 h period. The numerical predictions

closely match the analytical reference of 340 W, indicating consistent power generation irrespective of the diurnal variation in solar position. In contrast, the fixed planar PV system inclined at 30 °shows a parabolic power profile, rising from 0 W at 06:00 h to a maximum of approximately 295 W at solar noon (12:00 h), then declining to 0 W at 18:00 h. This behavior reflects the planar module's power output dependence on the changing angle of incidence of solar radiation throughout the day. Overall, the results indicate that the spherical configuration provides a higher and more consistent power output than the fixed planar configuration under the investigated modeling conditions.

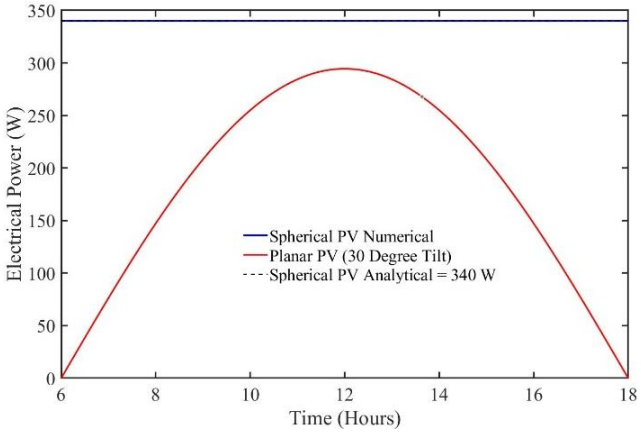

Figure 12. *Comparison of spherical with planar tilt at 30 degrees.*

The numerical results demonstrate close agreement between the numerically integrated and analytically determined projected area and electrical power over the simulation period of 06:00–18:00 h, as shown in Figure 13 and Figure 14. The projected area fluctuates slightly around the analytical value of 1.7 m ², with deviations of approximately 10-4 m ². Similarly, the numerical electrical power remains within 339.988–340.014 W, closely matching the analytical value of 340 W, with a maximum relative deviation of approximately 0.0044%.

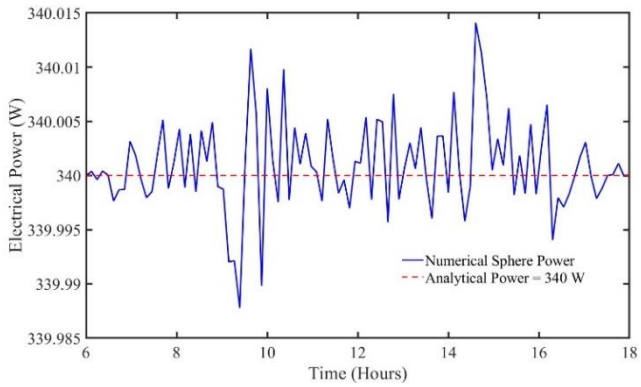

Figure 13. *Numerical and Analytical Spherical PV Power.*

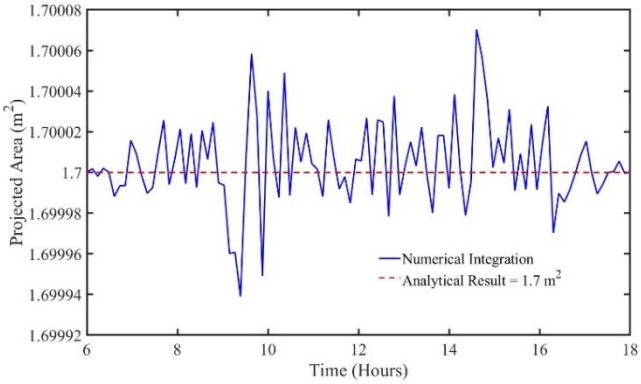

Figure 14. *Numerical and Analytical Spherical Projected Area.*

3.10. Limitation and Future Work

3.10.1. Limitations of the Electrical Model

The present study does not model the electrical interconnection of the discretized photovoltaic elements. Consequently, the effects of series–parallel wiring, current mismatch, bypass diode operation, nonlinear current–voltage characteristics, and maximum power point tracking are not considered. The reported power values therefore represent theoretical geometric energy capture rather than the expected output of a physically interconnected spherical photovoltaic module.

3.10.2. Future Work

Future work should be conducted to investigate practical electrical architectures for spherical photovoltaic systems, including electrical interconnection, cell mismatch, temperature effects, external shading, and maximum power point tracking (MPPT). Future studies should incorporate established astronomical solar position algorithms, such as the NREL Solar Position Algorithm, to better represent low solar elevation angles and seasonal variations. Experimental validation using physical PV prototypes is also recommended to establish the practical performance of spherical and planar configurations under real operating conditions.

Furthermore, although the complete spherical geometry demonstrated improved theoretical irradiance capture in the present simulation, its practical implementation requires consideration of photovoltaic material utilization and manufacturing costs. Since the lower hemisphere generally receives limited direct solar irradiance, its contribution to total energy generation may not justify the additional photovoltaic material required. Consequently, hemispherical or partially enclosed photovoltaic configurations may offer a more favourable balance between energy production and system cost. Future research should therefore undertake comparative techno-economic and energy-performance assessments of spherical, hemispherical, and planar photovoltaic configurations.

Future work should also extend the numerical convergence analysis to higher surface discretization resolutions (e.g.,

N=600 and beyond) to quantify integration accuracy and establish mesh-independent solutions. Further investigations should also evaluate the sensitivity of the predicted electrical power to surface discretization and temporal integration steps, strengthening confidence in the model's numerical accuracy, stability, and computational efficiency.

4. Conclusion

1) This study presented a comparative assessment of planar and spherical photovoltaic (PV) geometries, focusing on their irradiance capture behavior and theoretical total energy yield over a representative daylight cycle, with emphasis on the role of geometric configuration in system performance.
2) The planar PV system exhibited the expected angle-dependent response, characterized by a bell-shaped power profile, with peak output near solar noon and lower performance during morning and evening hours due to changes in solar incidence angle and the directional nature of the fixed surface. This established behavior was used as the baseline for comparison.
3) In contrast, the spherical PV system delivered near-constant theoretical power output throughout the modeled daylight period (approximately 340–343 W), resulting from its multi-orientational geometry that enables continuous theoretical solar irradiance capture across varying sun positions. This result is based on an idealized geometric model and does not include electrical interconnection effects, partial shading, mismatch losses, nonlinear current–voltage behavior, temperature effects, or maximum power point tracking.
4) Overall, the simulation results indicate that spherical photovoltaic geometry can improve theoretical irradiance capture under idealized conditions. Experimental validation and detailed electrical modeling are required before these theoretical advantages can be confirmed for practical photovoltaic systems. While the complete spherical geometry provides a useful theoretical benchmark for omnidirectional irradiance capture, future work should investigate hemispherical and other partially curved photovoltaic configurations to improve practical feasibility and reduce manufacturing cost.

Abbreviations

PV	Photovoltaic
MATLAB	Matrix Laboratory
G	Solar Irradiance

Author Contributions

Nyemo Ngambusu: Conceptualization, Resources, Writing – review & editing

Reginald Raphael: Data curation, Formal Analysis, Investigation, Methodology, Software, Visualization, Writing – original draft

Edward Dema: Data curation, Investigation, Validation, Writing – review & editing

Nyanda Madili Malashi: Conceptualization, Formal Analysis, Methodology, Project administration, Supervision, Writing – review & editing

Conflicts of Interest

The authors declare no conflicts of interest.

References

[1] Abdulmouti, H. (2025). Enhancing Power Generation: PIV Analysis of Flow Structures' Impact on Concentrated Solar Sphere Parameters. Energies, 18(12), 3162. https://doi.org/10.3390/en18123162

[2] Allouhi, A., Rehman, S., Buker, M. S., & Said, Z. (2022). Up-to-date literature review on Solar PV systems: Technology progress, market status and R&D. *Journal of Cleaner Production*, *362*, 132339. https://doi.org/10.1016/j.jclepro.2022.132339

[3] Ayed, H., Moria, H., Aldawi, F., Farouk, N., Sharma, K., Youshanlouei, M. M, Jarad, F. (2021). Thermal, efficiency and power output evaluation of pyramid, hexagonal and conical forms as solar panel. *Case Studies in Thermal Engineering*, *27*, 101232. https://doi.org/10.1016/j.csite.2021.101232

[4] BAÑUELOS, M. I. F. (2018). Method to Calculate the Electricity Generated by a Photovoltaic Cell, Based on Its Mathematical Model Simulations in MATLAB.

[5] Biancardo, M., Taira, K., Kogo, N., Kikuchi, H., Kumagai, N., Kuratani, N, Nakata, J. (2007). Characterization of microspherical semi-transparent solar cells and modules. *Solar Energy*, *81*(6), 711-716. https://doi.org/10.1016/j.solener.2006.10.009

[6] Dhimish, M., & Silvestre, S. (2019). Estimating the impact of azimuth-angle variations on photovoltaic annual energy production. *Clean Energy*, *3*(1), 47-58. https://doi.org/10.1093/ce/zky022

[7] Duffie, J. A., & Beckman, W. A. (2013). Solar engineering of thermal processes (4th ed.). John Wiley & Sons. https://doi.org/10.1002/9781118671603

[8] Eperon, G. E., Hörantner, M. T., & Snaith, H. J. (2017). Metal halide perovskite tandem and multiple-junction photovoltaics. *Nature Reviews Chemistry*, *1*(12), 0095. https://doi.org/10.1038/s41570-017-0095

[9] Green, M. A. (2016). Commercial progress and challenges for photovoltaics. *Nature Energy*, *1*(1), 15015. https://doi.org/10.1038/nenergy.2015.15

[10] Hossain, M. I., Qarony, W., Ma, S., Zeng, L., Knipp, D., & Tsang, Y. H. (2019). Perovskite/Silicon Tandem Solar Cells: From Detailed Balance Limit Calculations to Photon Management. *Nano-Micro Letters*, *11*(1), 58. https://doi.org/10.1007/s40820-019-0287-8

[11] Huang, B.-J., Huang, Y.-C., Chen, G.-Y., Hsu, P.-C., & Li, K. (2013). Improving Solar PV System Efficiency Using One-Axis 3-Position Sun Tracking. *Energy Procedia*, *33*, 280-287. https://doi.org/10.1016/j.egypro.2013.05.069

[12] IEA. (2024). Renewables 2023. IEA, Paris. https://www.iea.org/reports/renewables-2023 Licence: CC BY.

[13] Jamal, J., Mansur, I., Rasid, A., Mulyadi, M., Dihyah Marwan, M., & Marwan, M. (2024). Evaluating the shading effect of photovoltaic panels to optimize the performance ratio of a solar power system. *Results in Engineering*, *21*, 101878. https://doi.org/10.1016/j.rineng.2024.101878

[14] Klemun, M. M., Kavlak, G., McNerney, J., & Trancik, J. E. (2023). Mechanisms of hardware and soft technology evolution and the implications for solar energy cost trends. *Nature Energy*, *8*(8), 827-838. https://doi.org/10.1038/s41560-023-01286-9

[15] Klugmann-Radziemska, E. (2026). Environmental and Operational Factors That Affect the Performance of a Photovoltaic System. Energies, 19(3), 602. https://doi.org/10.3390/en19030602

[16] Martin, N., & Ruiz, J. M. (2001). Calculation of the PV modules angular losses under field conditions by means of an analytical model. Solar Energy Materials and Solar Cells, 70(1), 25-38. https://doi.org/10.1016/S0927-0248(00)00408-6

[17] Nelson, V. C. (2011). *Introduction to renewable energy*. CRC press.

[18] Pande, J., & Nasikkar, P. (2023). A Maximum Power Point Tracking Technique for a Wind Power System Based on the Trapezoidal Rule. Energies, 16(6), 2799. https://doi.org/10.3390/en16062799

[19] Rós-Ledesma, F., Barrutia, L., Ramírez-Ledesma, J., Narvarte, L., & Lorenzo, E. (2026). Angular losses in photovoltaic energy estimation: A review of models and a comparative analysis using the enhanced SISIFO simulation tool. *Renewable and Sustainable Energy Reviews*, *226*, 116377. https://doi.org/10.1016/j.rser.2025.116377

[20] Twidell, J. (2021). *Renewable energy resources*. Routledge.

[21] Ur Rahman, R., Yousuf, E. H., Alamgeer, Khokhar, M., & Yi, J. (2026). Efficiency enhancement in spherical solar cells through recombination control and carrier transport improvement. *Solar Energy*, *311*, 114518. https://doi.org/10.1016/j.solener.2026.114518

[22] Velasquez, P., Herrera, C., & Santis, A. (2021). Simulation of the Effect of the Angle of Incidence on the Solar Panel for Three Solar Photovoltaic (PV) Systems in the Bogotá Savanna–Subparamo. Chemical Engineering Transactions, 86, 739–744. https://doi.org/10.3303/CET2186124

[23] Vermaak, H. J. (2014). Techno-economic Analysis of Solar Tracking Systems in South Africa. *Energy Procedia*, *61*, 2435-2438. https://doi.org/10.1016/j.egypro.2014.12.018

[24] Wang, K., Zheng, J., Yu, R., & Tan, Z. A. (2025). Recent Progress on High-Efficiency Perovskite/Organic Tandem Solar Cells. Nanomaterials, 15(10), 745. https://doi.org/10.3390/nano15100745

[25] Zhu, Z., Mao, K., & Xu, J. (2021). Perovskite tandem solar cells with improved efficiency and stability. *Journal of Energy Chemistry*, *58*, 219-232. https://doi.org/10.1016/j.jechem.2020.09.022

[26] F. Nicoletti, M. A. Cucumo, V. Ferraro, D. Kaliakatsos, and J. Settino, "Performance Analysis of a Double-Sided PV Plant Oriented with Backtracking System," *Math. Model. Eng. Probl.*, vol. 7, no. 3, pp. 325–334, Sep. 2020, https://doi.org/10.18280/mmep.070301

[27] A. González, "Measurement of areas on a sphere using Fibonacci and latitude–longitude lattices," Mathematical Geosciences, 2009. https://doi.org/10.1007/s11004-009-9257-x

[28] D. Greenhalgh, Solar Energy Collection Using Spherical Photovoltaic Structures, Ph.D. thesis, University of Southampton, 2017. Access thesis.

[29] J. H. Hannay and J. F. Nye, "Fibonacci numerical integration on a sphere," Journal of Physics A: Mathematical and General, vol. 37, no. 48, pp. 11591–11601, 2004. https://doi.org/10.1088/0305-4470/37/48/005

[30] National Renewable Energy Laboratory (NREL), Reference Cell Performance and Calibration, 2023. Access technical report.

[31] K. K. Stevens, "On the response of linear systems to modulated sinusoidal inputs," Journal of Sound and Vibration, vol. 21, no. 3, pp. 295–306, 1972. https://doi.org/10.1016/0022-460X(72)90814-0